How to Cite:
Al-Niaimi, A. F. D., & Mahmood, E. I. (2022). Removal of methyl orange dye using(ZnO/MWCNTs) nanomaterial. *International Journal of Health Sciences*, *6*(S3), 10138–10155. https://doi.org/10.53730/ijhs.v6nS3.9371

Removal of methyl orange dye using (ZnO/MWCNTs) nanomaterial

Amir Fahdil Dawood Al-Niaimi
Depatment of Chemistry, College of Science, University of Diyala, Diyala, Iraq

Esraa Ibraheim Mahmood
Depatment of Chemistry, College of Science, University of Diyala, Diyala, Iraq

***Abstract*---**The (ZnO/MWCNTs) Nano composite had a composition of (0.8/0.018MWCNTs) (w/w). Batch adsorption method was used to remove Methyl orang dye from its aqueous solution. The structural characteristics of (ZnO/MWCNTs) were investigated (FTIR, XRD, BET, EDX, FE-SEM). The (ZnO) was discovered to have a 22 nm average particle size with surface area (27. 71$m^2.g^{-1}$). The (ZnO/MWCNTs) was discovered to have a surface area (38. 85$m^2.g^{-1}$.). Adsorption equilibrium data was fitted with, Temkin equations to describe the isotherms, more than Freundlich, and Langmuir and Dubinin-Radushkevich isotherms. Thermodynamic studies showed that the adsorption was exothermic and spontaneous and pysisorption nature of adsorption. The pseudo-first and second order models were used to fit the kinetic data, adsorption process flow the pseudo-second-order adsorption.

***Keywords*---**methyl orange, nanomaterial, exothermic.

Introduction

Dyes are widely used in industries including textile, printing, plastic, pharmaceutical, leather, paper and a food processing [1]. The waste water of industrial activities contains a variety of potentially toxic and environmentally harmful compounds[2]. The most dyes are stable to light and oxidizing agents in nature[3] Pesticides, phenols, amines, and aromatic amines are the most frequent organic pollutants that contribute to environmental pollution [4]. The most common adsorbents utilized to remove pollutants include carbon, zeolites and polymers, bulk, siliceous materials, agricultural waste, and industrial waste [5] [6]. The high surface area, well-developed pore structure, and presence of functional groups on the surface of activated carbon make them ideal adsorbents [7] [8]. A higher removal % of both water-soluble and insoluble pollutants, even at lower concentrations of pollutants, the ability to regenerate adsorbents, as well as

the ability to utilize it in batch or continuous mode, are all advantages of utilizing activated carbon adsorption [9]10]. Of all the physical, chemical and biological treating strategies, adsorption still remains the most simple, low cost and most effective treatment for dye effluents[11]. Less research has been done on the effects of impregnating or loading activated carbon with metals to improve organic pollutant adsorption. Electrostatic interactions between metals or metal oxides loaded onto the surface of a carbon nano tube may increase the adsorption of anionic organic pollutants.

Material and Method

Chemicals

MO (purity >97%) was purchased from Merck (Darmstadt, Germany) as a commercially available dye without any further purification. The dye's chemical structure and its main characteristics are shown in fig1. Solutions were prepared using bidistilled water.[12],A UV–Vis spectrophotometer (Shimadzu UV Spectrophotometer) was used to measure the residual concentration of MO at a wavelength of 463.8 nm. The absorbance was found to fluctuate linearly with concentration according to the Lambert-Beer rule, and the calibration curve is displayed in Figure 2. zinc nitrate trihydrate ($ZnO(NO_3).3H2O$) and sodium bicarbonate ($NaHCO_3$) It was used as raw materials for the preparation of ZnO nanoparticles.

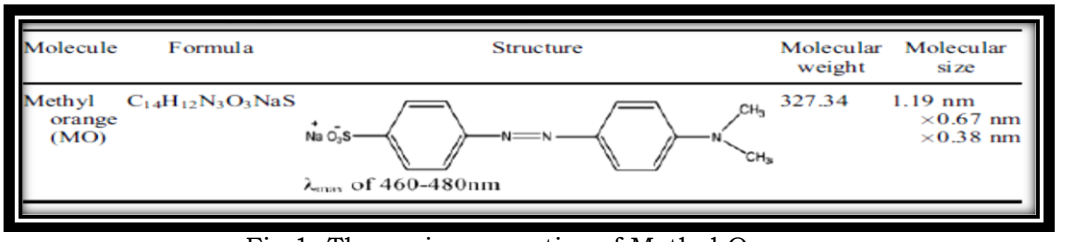

Fig 1. The main properties of Methyl Orang

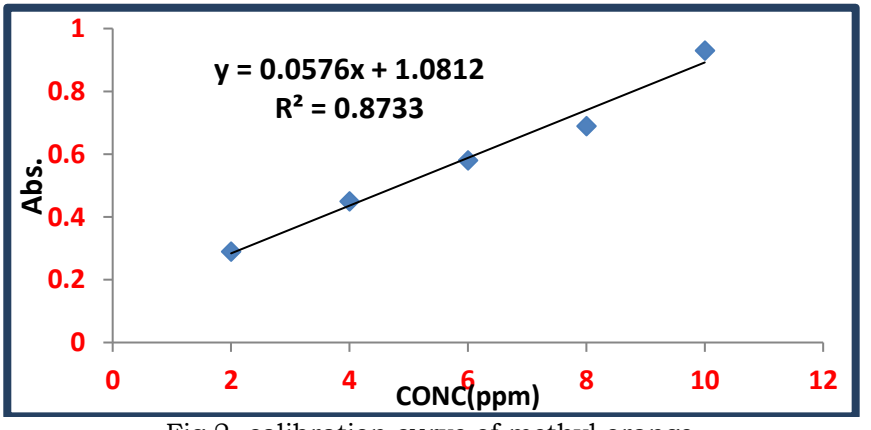

Fig 2. calibration curve of methyl orange

Preparation of zin oxide nanoparticles

The zinc oxide ZnO nanoparticles were generated using a simple precipitation procedure in which (0.2M) of zinc nitrate trihydrate (ZnO (NO_3).3H2O) and (0.4M) sodium bicarbonate (NaHCO3) were mixed separately in 100 ml of distilled water and agitated for half an hour. The sodium bicarbonate aqueous solution was progressively added to the zinc nitrate aqueous solution with continuous mixing and at a temperature of 50 °C until the pH of the combination reached 6.8.After that, the process produced white precipitated particles. To eliminate the bicarbonate residue, the zinc oxide particles were filtered and rinsed with distilled water multiple times before being dried in the air for two hours at 80 degrees. To make ZnO nanoparticles, the final powder is calcined for three hours at 400 °C under air. [13]

Preparation of (ZnO/MWCNTs) nanocoposite

The nano Zinc oxide (ZnO 0.8gm) was loaded onto (MWCNTs 0.018g) in an ethanol solution to form the (ZnO/MWCNTs) nanocomposite. Before mixing, multiwalled carbon nanotubes were activated using hydrogen peroxide and ammonia.

Characterizations results

Fourier-transform Infrared (FTIR)
Fourier Transform Infrared Spectroscopy of (ZnO)

The infrared spectrum is shown in Figure (3), which is due to nano-zinc oxide. It shows an absorption band at the wave number of (3470.82)cm^{-1}, indicating the presence of the stretch hydroxyl group belonging to the water molecule, while the apparent absorption bands at (1494.36) cm^{-1},refer to the presence of a (C-C) group, while the absorption bands (1127.14) cm^{-1}, belong to the (C-O) group, and the absorption bands in the fingerprint area below (1000) cm^{-1}, belong to Zn-O at (709.95) cm^{-1}, (549.11) cm^{-1}. [14]

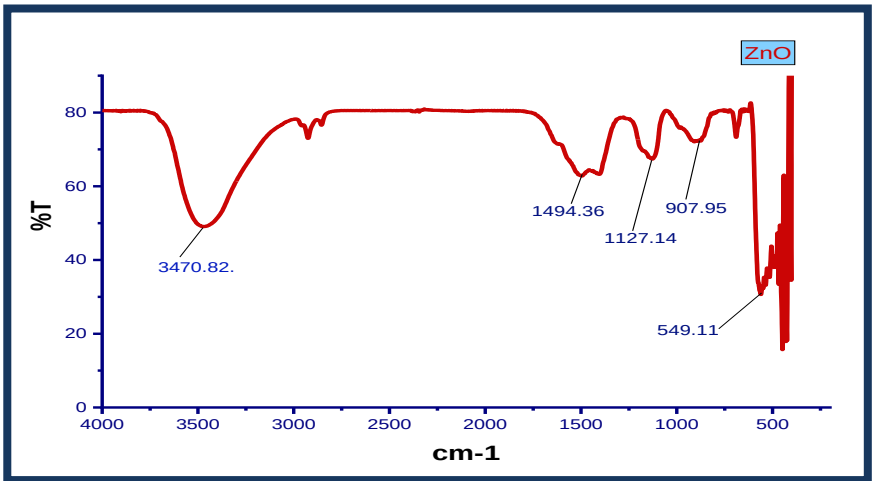

Fig 3. Fourier Transform Infrared Spectroscopy of (ZnO)

Fourier Transform Infrared Spectroscopy of (MWCNTs)

Figure (4) shows the appearance of a number of bands, where a band appears at (3398.15) cm^{-1}, which belongs to the (OH) groups, while the band that appears at (2922.78)cm^{-1} belongs to group (C-H), as it appeared Another band at (1645.21)cm^{-1} is due to the stretching of the bond (C-O) of the carbonyl group of multi-walled carbon nano tubes. The appearance of the band (1645,21)cm^{-1} indicates the activation process of the MWCNTs, in addition to the presence of the fundemantul band at (3398.15)cm^{-1}.[15]

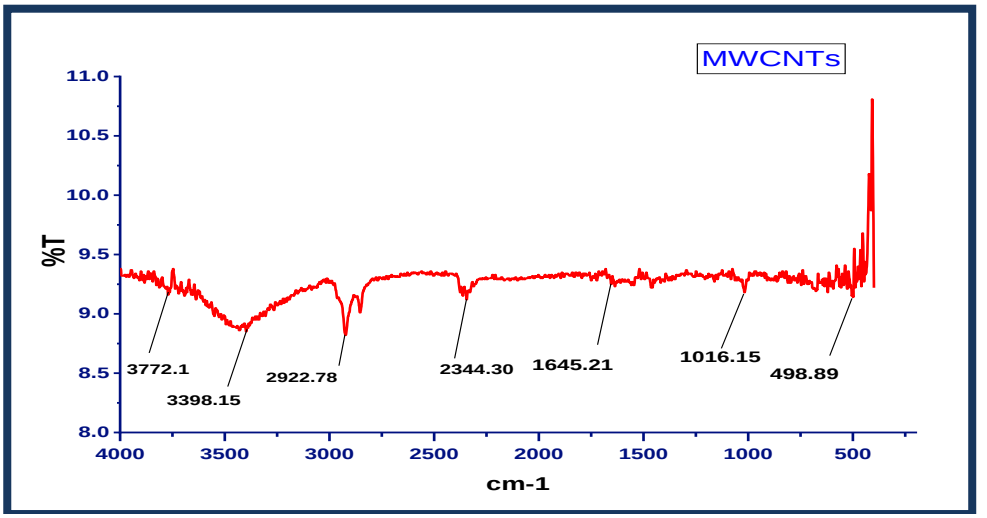

Fig 4. Fourier Transform Infrared Spectroscopy of (MWCNTs)

Fourier Transform Infrared Spectroscopy of (ZnO/MWCNTs)

The infrared spectrum shown in Figure (5), which is due to the (ZnO/MWCNTs), shows absorption bands at 1 2916.5 cm-1 (3470.82) cm and (417.2) cm-1 due to the basic bands of the zinc oxide [16], either The absorption bands that appear at (1528.6) cm-1 and (1135.4) cm-1 belong to the (C=C) and (C-H) groups of carbon nano tubes [17], while the absorption band cn1(3518.2)cm-1 appears at a higher frequency for the same group for each of the two components of the complex, which belongs to the hydroxyl group is attached to zinc oxide (ZnO) and the second band at (3470.82)cm-1 appears in the region of high frequencies that belong to the (OH) group linked to the surfaces of multi-walled carbon nanotubes. The displacement of these frequencies to higher values is due to the interference between those effective groups. This indicates the mixing of zinc oxide particles with the multi-walled carbon nano tubes.

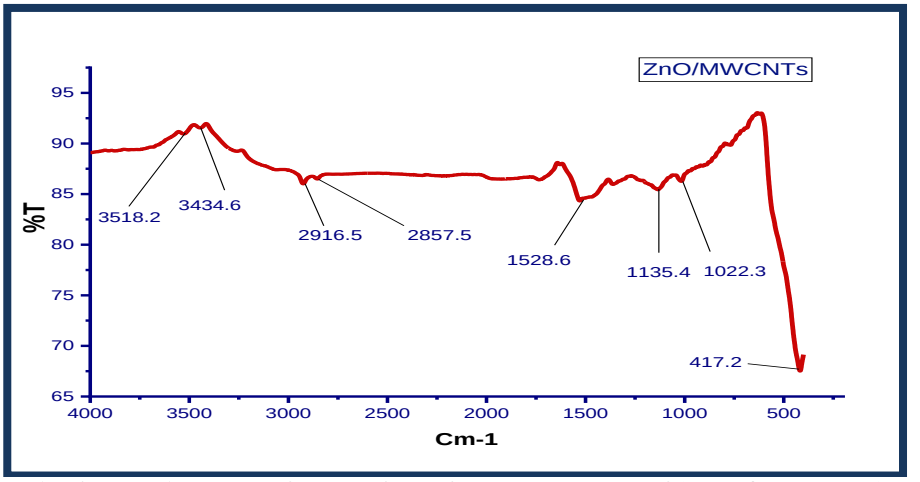

Fig 5. Fourier Transform Infrared Spectroscopy of (ZnO/MWCNTs)

Structure analysis by XRD
X-ray diffraction of ZNO

The results of the X-ray examinations for nanopartical zinc oxide, which are shown in Figure (6), showed that the highest values were obtained for the diffraction angles (2,31.8,34.4,36) corresponding to Miller's coefficients (101,100,002), which correspond to what was mentioned in the card with the number (2551-070-01). It has been shown from the figure below that the prepared nanopartical zinc oxide is in the form of a sharp section, and the crystal growth is of high purity because no overlapping funnel appears, and that the size of the nanopartical grains obtained is 22 mm. [18]

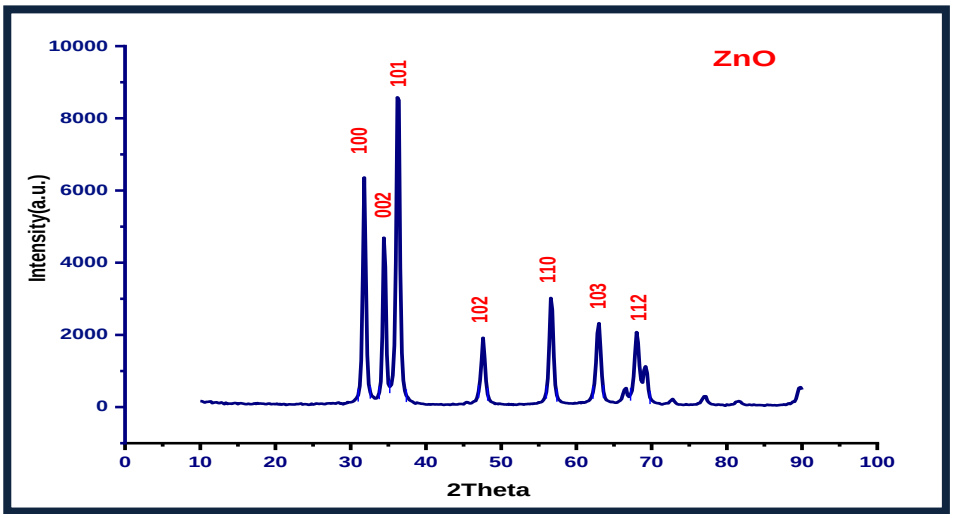

Fig 6. X-ray diffraction of ZNO

X-ray diffraction of ZNO/MWCNT

In order to comprehend the composite's structure (MWCNTs/ZnO), the XRD pattern of MWCNTS loaded with ZnO nanoparticles is shown in Figure (7). The peak (26.4) may be noticed as a result of Miller's modulus (002) of (MWCNTs). [19] while the other peaks of the compound significant feature corresponds to hexagonal ZnO. (JCPDS card number 79-0205) [20]. The presence of a pure phase in ZnO was confirmed by XRD pattern, with no sections containing additional impurities, indicating that the compound comprised pure ZnO. The sharp peaks revealed that zinc oxide in the sample had crystallized well [30]. The size of the nanoparticales composite (ZnO/MWCNTs) was estimated based on the Debbai Scherer equation, which is about 13 nm.

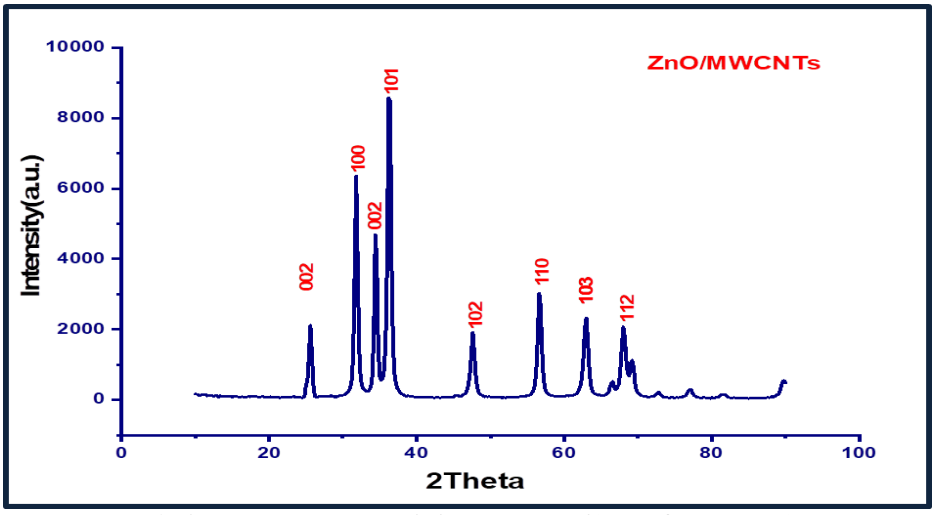

Fig 7. XRD pattern of the prepared(ZnO/ MWCNT)

Analysis of nanomaterials' using an FE-SEM and EDX

Figure (8-a) shows that the surface of (MWCNTs) is covered with layers of nanoparticular ZnO [21], and it is noted in Figure (8-b) that the structure is network-like in which the nanoparticles of ZnO NPs are embedded on the surface of MWCNTs and form bonds with functional groups on the MWCNT surface. Moreover, the properties of ZnO NPs and ZnO/MWCNTs were explored using energy-dispersive X-ray (EDX) that identifies the elements in the sample. [22] As in Fig. (9).The results show that the sample contains Zn.O.C and also show the formation of ZnO/MWCNTs. The two pictures (a and b) show the zinc oxide material, which has the largest proportion. Despite this, the carbon nanotubes are clearly visible in the picture (b) despite the small amount that was used in preparing the composite. And the smallest diameter obtained is (19.91.29.58) nm.

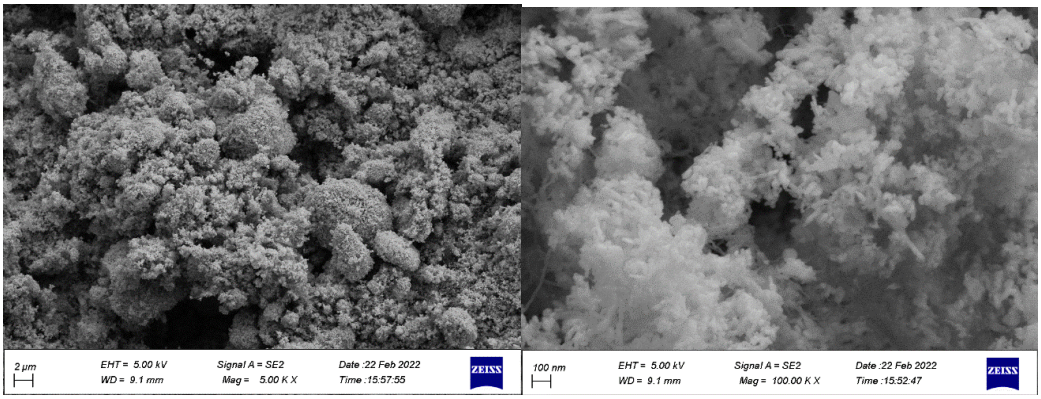

Fig 8. (a,b)FE-SEM of (ZnO/MWCNTs)

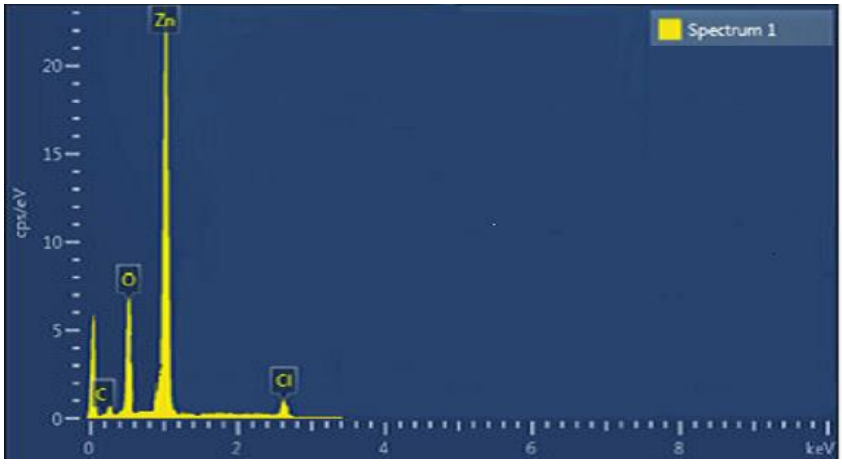

Fig 9. EDX of the prepared MWCNT/ZNO

Adsorption Results

Effect of time

As shown in figure 10, the contact time is one of the most critical parameters for modeling and developing the adsorption process in industry [23]. Figure10 shows that the majority of dye sorption occurred in the first 30 minutes. The rapid sorption rate was owing to the fact that the adsorbent surface had all of its active sites empty and the solution concentration was high at the beginning. Due to the interactions between the solute molecules of the solid and the bulk phase, only a very small increase is noticed in metal uptake after that point [24]

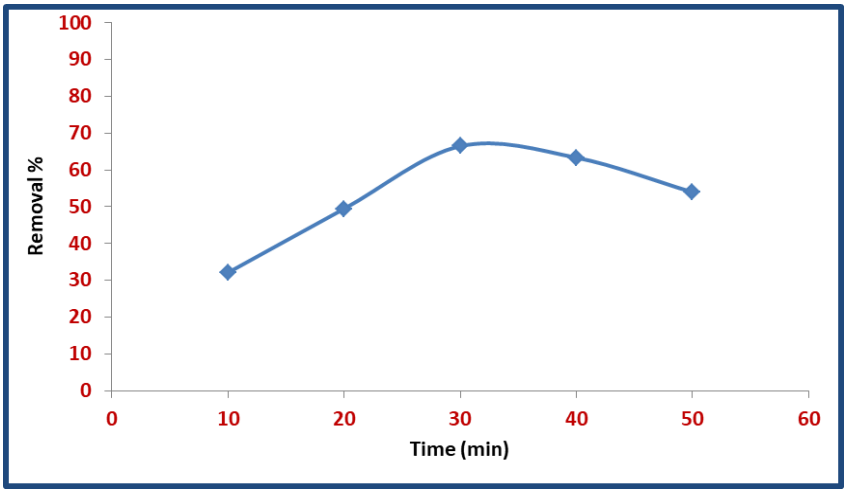

Fig 10. Effect of contect time

Effect of mass dosage

Figure 11 depicts the effect of adsorbent dosage (mass) on methyl orange dye adsorption. Many factors influence the process, but dosage is likely the most important since it controls the capacity of the sorbent at a particular starting concentration. By increasing the quantity of (ZNO/MWCNT), the pollutants can be totally adsorb or approach equilibrium at a given concentration of each pollutant. When there were enough initial binding sites for contaminant complexation. The observed result occurred because, when the dosage was increased beyond the reference points, an equilibrium was established between the pollutants bound to the sorbent and those that remained unabsorbed in the mixture. Low mass doses resulted in a higher qe value, which led in pollutant saturation occurring more quickly. An increase in lower energy sites occupied leads in a lower qe value, but this drop in energy is countered by an increase in the percentage of higher energy sites filled. [25]

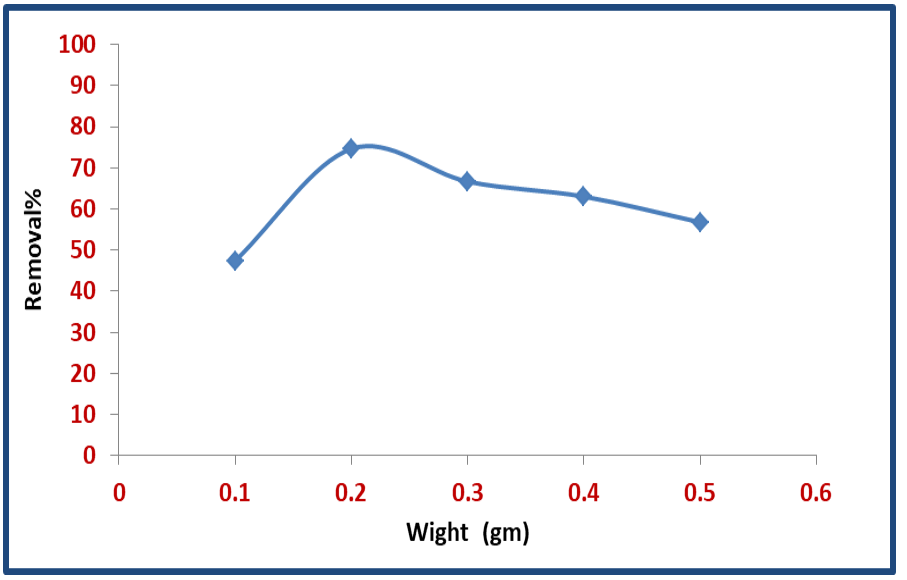

Fig 11. Effect of adsorbent dos on the removal percentage

Effect of initial concentration

In order to overcome all of the mass transfer resistance between the aqueous and solid phases, the initial concentration offers a significant driving force[26] as shown in figure12. Initial methyle orange concentrations ranged from 10 to 50 ppm for these tests.

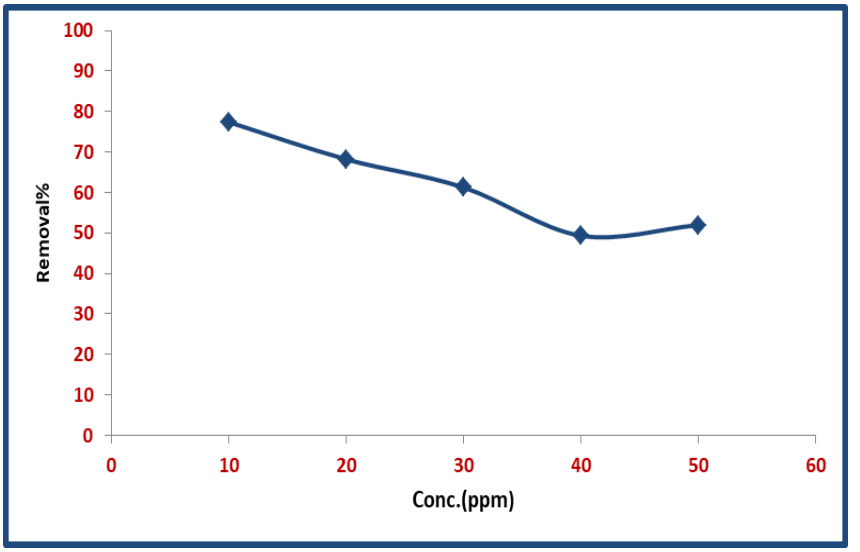

Fig 12. Effect of MO Concentration

Effect of PH

By varying the acid function within the range (3–11) PH, the influence of the acid function on the adsorption process of methyl orange dye on the surface of the composite (ZnO/MWCNTs) was investigated, as the experiment was carried out at the appropriate weight and time for the dye. Figure 13 illustrates the acquired results. The dye was removed from its aqueous solution with the greatest efficiency at pH = 5, which promotes adsorption owing to ionization of the surface and deprotonation of the dye MO. This results in the proper methyl orange adsorption. Negatively charged forms bind to the surface's active spots. [27] The decrease in adsorption with rising pH is owing to an increase in hydroxide ion deposition and, as a result, the concentration of negative charges on the surface, which lowers MO adsorption. [28]

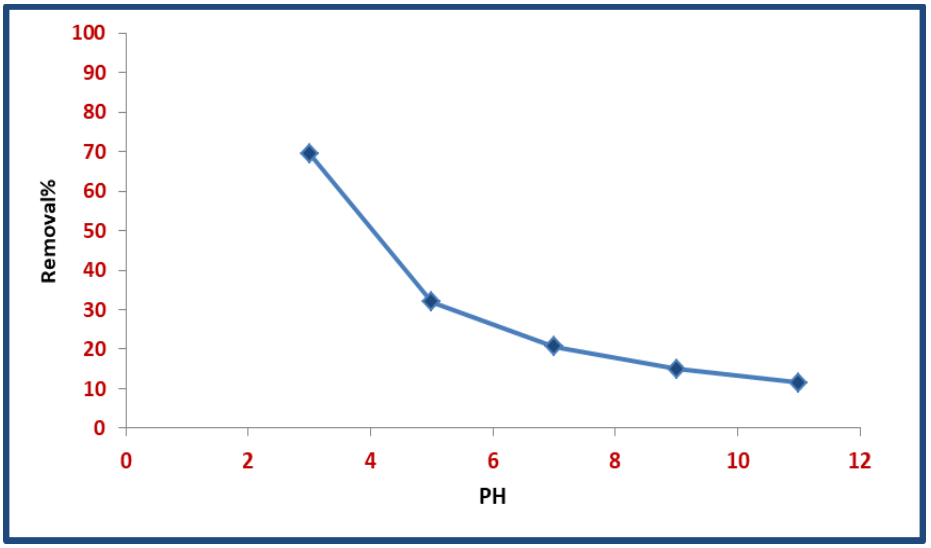

Fig 13. Effect of PH

Adsorption kinetic

As illustrated in figure 15, adsorption kinetics specifies the rate of adsorbate absorption on the adsorbent, which influences the adsorption equilibrium time (a,b). Modeling the adsorption process requires an understanding of adsorption kinetics. The experimental results of the ZNO/MWCNTs methyl orange adsorption were analyzed using pseudo-first-order and pseudo-second-order adsorption kinetic models. The adsorption process is consistent with both pseudo-first-order and pseudo-second-order kinetics, as shown in the diagram below, although it is more compatible with pseudo-second-order kinetics.

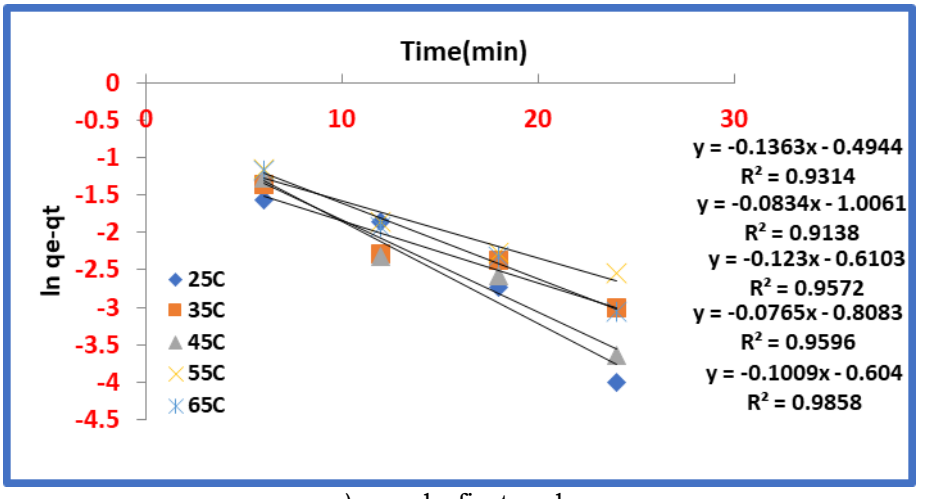

a)pesudo-first-order

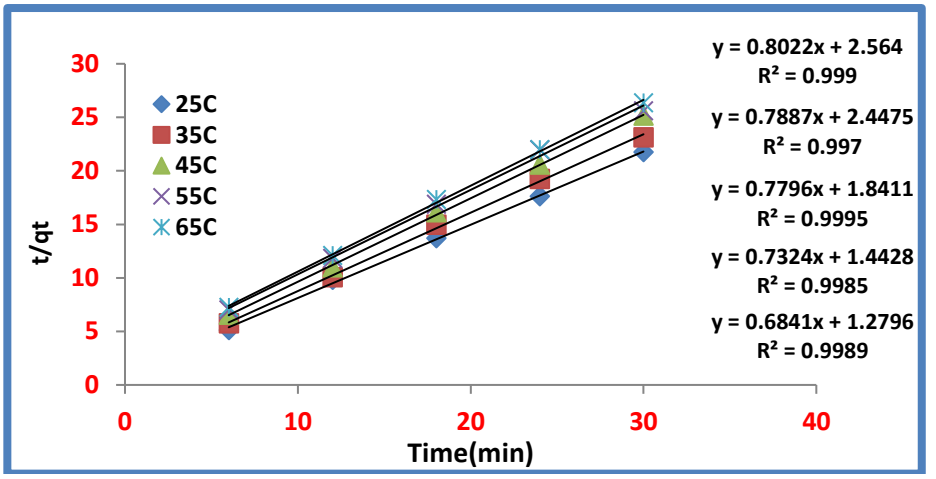

b)pesudo-second-order

Figure 15. (a-b) adsorption kinetic model first and second order

Table 1
Adsorption kinetic parameters model first and second order

C0	TC	Pseudo-First-order			Pseudo-Second-order		
		K1 Min-1	qe calc	R^2	K2 ($g.mg^{-1}.min$)	qe calc	R^2
10ppm	25	0.136	0.609	0.934	0.250	1.246	0.999
	35	0.083	0.365	0.913	0.253	1.269	0.997
	45	0.123	0.543	0.957	0.329	1.283	0.999
	55	0.076	0.445	0.959	0.371	1.366	0.998
	65	0.1	0.546	0.985	0.365	1.461	0.998

Adsorption isotherm

Under certain conditions, the term "adsorption isotherm" is used to describe the relationship between adsorbate concentration in solution (liquid phase) and adsorbent concentration in solid phase at a constant temperature [29]. Three distinct adsorption isotherm models were used to analyze the equilibrium adsorption data: Langmuir, Freundlich, and Temkin. To characterize the isotherms, it was fitted utilizing Temkin equations with highest values of correlation coefficient.

Langmuir

According to this notion, adsorption occurs in a monolayer, and all adsorption sites on the adsorbent are homogenous. It is expressed using a linear equation[30].

$$Ce/Qe = 1/kLQmax + Ce/Qmax \quad \ldots(1)$$

The maximum adsorption efficiency is Qm (mg.g-1), and the dependency-constant is KL (L.mg-1). The maximum adsorption efficiency and Langmuir constant will be calculated using the slope and intercept of the linear plots Ce/Qe vs Ce, resulting in a straight line with a slope of 1/Qmax that is consistent with full monolayer coverage (mg.g-1), while the intercept reflects the number 1/kLQmax.

Freundlich

It is one of the most essential isotherms for studying adsorption from a solution, especially in a non-ideal system. This concept claims that materials adsorb on heterogeneous surfaces (Hetro-surfaces) and that the attractiveness of the adsorption sites held by the adsorbing surface varies from one site to the next. Also, because of the varied adsorption sites in terms of their energy levels, this sort of adsorption isotherm is multi-layered rather than single-layered, and the Frendelich linear connection is mathematically stated in the following manner[31].

$$\ln qe = \ln KF + \frac{1}{n}\ln Ce \quad (2)$$

KF and n are constants that represent adsorption capacity and intensity, respectively.

Temkin

This form of isotherm assumes that the adsorption process is influenced by indirect influences. Because the heat of adsorption is greatly affected by the process of overlap between the adsorbent surface and the adsorbent material, the higher the coverage, the lower the adsorption heat in a linear manner for all those layers, and the linear mathematical relationship that expresses an equation that can be as follows[32].

$$q_e = B_T \ln K_T + B_T \ln C_e \quad (3)$$

B=RT/bT, where bT (J/mol) is the adsorption heat, AT or (KT) (L/g) is the Temkin isotherm equilibrium binding constant, R is the gas constant (8.314 J/mol.K), and T is the absolute temperature at Kelvin. The slope and intercept of the plot of Qe versus ln Ce may be used to calculate the values of B and AT.

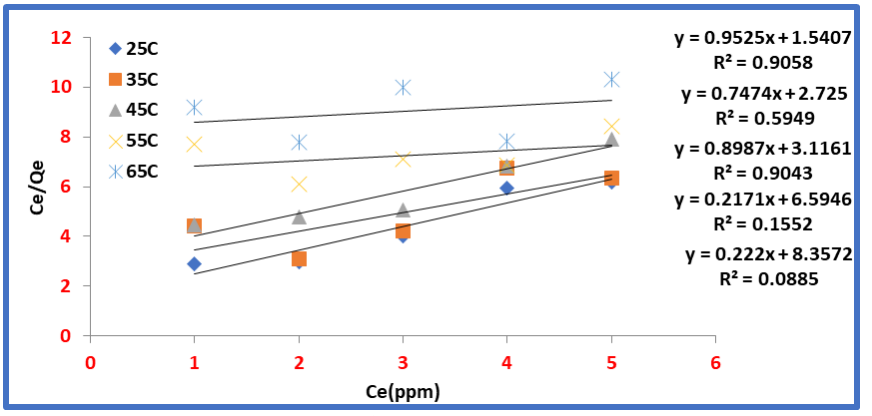

a) Langmur

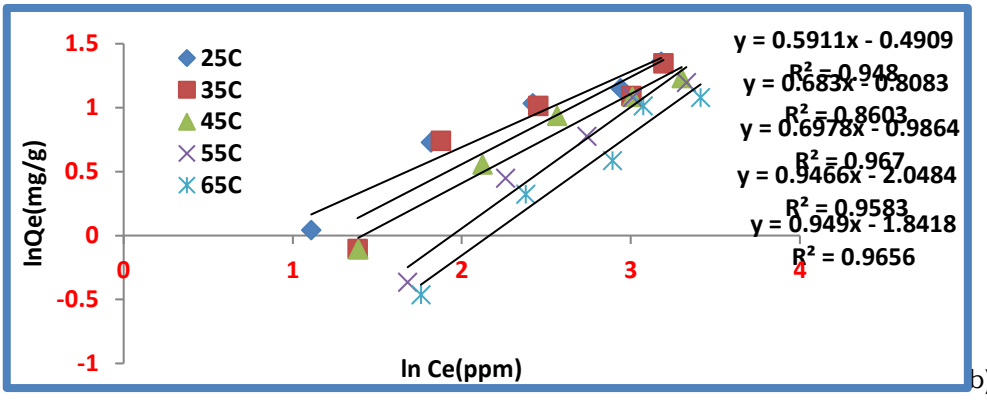

b) Freundlich

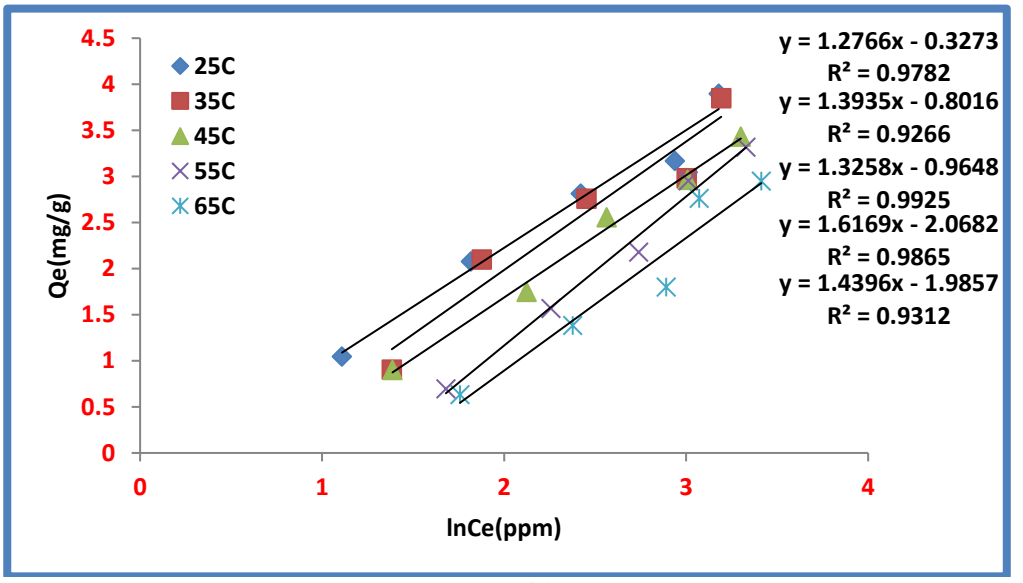

c) Temkin

Fig 16. adsorption isotherm models a,b,c

Table 2
Isotherms parameter

				Langmuir		Freundlich		
TC	R^2	KL	Qmax	RL	R^2	n	KF	
25	0.905	0.618	1.050	0.139	0.948	1.692	0.612	
35	0.594	0.274	1.338	0.267	0.86	1.464	0.445	
45	0.904	0.288	1.113	0.257	0.967	1.434	0.373	
55	0.155	0.032	4.608	0.752	0.958	1.057	0.128	
65	0.088	0.026	4.504	0.790	0.965	1.053	0.158	
				DKR				Temkin
R^2	E	Qmax	ß		R^2	BT	KT	
0.945	0.455	3.340	2.415		0.978	1.276	0.773	
0.973	0.348	3.514	4.128		0.926	1.393	0.562	
0.93	0.370	3.022	3.643		0.992	1.325	0.483	
0.954	0.265	3.061	7.083		0.986	1.616	0.278	
0.911	0.258	2.643	7.481		0.931	1.439	0.251	

Thermodynamic study

The following equation was used to compute the thermodynamic parameter, enthalpy (ΔH).

$$K_C = Ae^{-\Delta H / RT} \quad (4)$$

$$\ln Xm = -\Delta H/RT + K \quad (5)$$

lnXm is the natural logarithm for the largest quantity adsorbed (mg/g), K is the Van't Hoff equation constant, R is the universal gas constant (8.314.10-3 kJ/mol. K-1), and T is the temperature (Kelvin). [32] [33], **Δ**G° may be calculated using Gibs' equation: [34]

$$\Delta G^\circ = -RT \ln Kc \qquad (6)$$

and **ΔS°** can be finde by equation

$$\Delta G^\circ = \Delta H - T\Delta S^\circ \qquad (7)$$

$$\Delta S^\circ = \frac{\Delta H - \Delta G^\circ}{T} \qquad (8)$$

proposed that Kc can be obtained as a dimensionless constant by multiplying K in (L/mg) by 10^6

$$Kc = K \times 10^6 \qquad (18)$$

$$\Delta G = -RT\ln(K \times 10^6) \qquad (19)$$

10^6 factor is assumed to be solution density taking the density of pure water to be 1.0 g/ml[35]. Table 2 depicts the calculated values of thermodynamic parameters of methyl orange adsorption on (ZnO/MWCNTs). The amount of the enthalpy change can be used to classify physical adsorption and chemisorption to some extent, Bonding strengths of 84 kJ/mol are thought to be typical of physical adsorption type bonds[36], Based on this, with an enthalpy of -5.87 KJ/mol, MO adsorption appears to be a physical adsorption process. the positive values of entropy variations showed that there was a random interference at the solid- a liquid interface during the fixation on the active sites of the adsorbent. The negative or nil values of Gibbs free energy (ΔG°) indicated the feasibility and spontaneity of the adsorption process without an induction period.[37]

Table 2
Thermodynamic parameter

C0	Thermodynamic Function	25Cº	35Cº	45Cº	55Cº	65Cº
50ppm	ΔG (KJ/mol)	-29.72	-30.65	-31.05	-31.86	-32.27
	ΔH (KJ/mol)	-5.87				
	ΔS (KJ/mol.k)	0.080	0.080	0.079	0.079	0.078

Conclusion

The investigation into the multiwall carbon nano tube that has been treated with ZnO has yielded a positive outcome. The results showed that 0.2 g of ZNO loading removed methyl orange. The efficacy of using (ZnO/MWCNTs) to remove Methyl Orang dye from aqueous solution was evaluated using batch adsorption testing. Temkin equations were used to fit the adsorption equilibrium data and characterize the isotherms. The kinetic data was fitted with 0.9 accuracy using

pseudo-second order models. MO adsorption looks to be a physical adsorption technique with the potential for spontaneity and practicality.

References

1. AL-Niaimi, A. F. D., Atiya, G. I., & Abdulateef, D. A. (2018). Thermodynamics and kinetic study of Eosin dye adsorption on CuO nanoparticles. International Journal of Research in Pharmacy and Chemistry, 8(2), 281–293. www.ijrpc.com
2. Fahdil A, AL-Niaimi D, O. A. (2018). Adsorption of Orange G Dye from Aqueous Solutions Using Magnesium Oxide Nanoparticles. Journal of Biochemical Technology, 9(3), 31-38.
3. Dawood, A., Adris, G., & Ahmed, D. (2019). Thermodynamic and Kinetic Study of the Eosin Dye Removal from Aqueous Solution by ZnO Nanoparticles. Diyala Journal For Pure Science, 15(1), 55–75.
4. Crini, G. (2006). Non-conventional low-cost adsorbents for dye removal: a review. Bioresource technology, 97(9), 1061-1085.
5. Iranmanesh, S., Harding, T., Abedi, J., Seyedeyn-Azad, F., & Layzell, D. B. (2014). Adsorption of naphthenic acids on high surface area activated carbons. Journal of Environmental Science and Health, Part A, 49(8), 913-922.
6. Huang, C. P., & Wu, M. H. (1977). The removal of chromium (VI) from dilute aqueous solution by activated carbon. Water Research, 11(8), 673-679.
7. Jiang, Z., Liu, Y., Sun, X., Tian, F., Sun, F., Liang, C., ... & Li, C. (2003). Activated carbons chemically modified by concentrated H2SO4 for the adsorption of the pollutants from wastewater and the dibenzothiophene from fuel oils. Langmuir, 19(3), 731-736.
8. Wang, S., Zhu, Z. H., Coomes, A., Haghseresht, F., & Lu, G. Q. (2005). The physical and surface chemical characteristics of activated carbons and the adsorption of methylene blue from wastewater. Journal of colloid and interface science, 284(2), 440-446.
9. Grover, D. P., Zhou, J. L., Frickers, P. E., & Readman, J. W. (2011). Improved removal of estrogenic and pharmaceutical compounds in sewage effluent by full scale granular activated carbon: Impact on receiving river water. Journal of Hazardous Materials, 185(2-3), 1005-1011.
10. Demirbas, A. (2009). Agricultural based activated carbons for the removal of dyes from aqueous solutions: a review. Journal of hazardous materials, 167(1-3), 1-9.
11. Al-niaimi, A. F. D., & Kamel, R. L. (2020). Adsorption and Optical Color Decomposition of Congo Red Blue Solution Using Graphene Oxide / MnO 2 Nano Composite. 11, 74–84.
12. Sprynskyy, M., Szczyglewska, P., Wojtczak, I., Nowak, I., Witkowski, A., Buszewski, B., & Feliczak-Guzik, A. (2021). Diatom Biosilica Doped with Palladium (II) Chloride Nanoparticles as New Efficient Photocatalysts for Methyl Orange Degradation. International journal of molecular sciences, 22(13), 6734.
13. Ali, Z. R., & Dawood AL-Niaimi, A. F. (2022). A Structural and Electrical characterizations of new synthesized PVA/PoPDA-rGO-ZnO Nano composite. Egyptian Journal of Chemistry, 65(4), 1-2.

14. Mubarak, T. H., Hassan, K. H., & Abbas, Z. M. A. (2013). Using X-ray diffraction and scanning electron microscope to study zinc oxide nanoparticles prepared by wet chemical method. In Advanced Materials Research (Vol. 685, pp. 119-122). Trans Tech Publications Ltd.
15. Dawood, A. F., & Khalil, M. A. A. K. (2022). Removal of basic fuchsine dye using (TiO2/MWCNTs) nanomaterial. Materials Today: Proceedings, 49, 2888-2897.
16. Violet, C., Franco, P., Sacco, O., & Marco, I. De. (2019). Zinc Oxide Nanoparticles Obtained by Supercritical Antisolvent Precipitation for the Photocatalytic.
17. Rafique, S., Bashir, S., Akram, R., Kiyani, F. B., Raza, S., Hussain, M., & Fatima, S. K. (2022). Variation in the Performance of MWCNT/ZnO Hybrid Material with pH for Efficient Antibacterial Agent. BioMed Research International, 2022.
18. Fernandez-Garcia, M., Martinez-Arias, A., Hanson, J. C., and Rodriguez, J. A. (2004). Nanostructured oxides in chemistry: characterization and properties. Chemical Reviews, 104(9), 4063-4104.
19. Morsy, M., Helal, M., El-Okr, M., & Ibrahim, M. (2014). Preparation, purification and characterization of high purity multi-wall carbon nanotube. Spectrochimica Acta - Part A: Molecular and Biomolecular Spectroscopy, 132, 594–598.
20. Aravinda, L. S., Nagaraja, K. K., Nagaraja, H. S., Bhat, K. U., & Bhat, B. R. (2013). ZnO/carbon nanotube nanocomposite for high energy density supercapacitors. Electrochimica Acta, 95(2010), 119–124.
21. Feng, W., Chen, J., & Hou, C. yan. (2014). Growth and characterization of ZnO needles. Applied Nanoscience (Switzerland), 4(1), 15–18.
22. 22- Saleh, T. A., Gondal, M. A., & Drmosh, Q. A. (2010). Preparation of a MWCNT/ZnO nanocomposite and its photocatalytic activity for the removal of cyanide from water using a laser. Nanotechnology, 21(49).
23. Franco, P., Sacco, O., De Marco, I., & Vaiano, V. (2019). Zinc oxide nanoparticles obtained by supercritical antisolvent precipitation for the photocatalytic degradation of crystal violet dye. Catalysts, 9(4), 346.
24. Sahebian, S., Zebarjad, S. M., & Lazzeri, A. (2015). A study on the dependence of structure of multi-walled carbon nanotubes on acid treatment. Journal of Nanostructure in Chemistry, 5(3), 287-293.
25. Sonune, A., & Ghate, R. (2004). Developments in wastewater treatment methods. Desalination, 167, 55-63.
26. Chen, Z. X., Jin, X. Y., Chen, Z., Megharaj, M., & Naidu, R. (2011). Removal of methyl orange from aqueous solution using bentonite-supported nanoscale zero-valent iron. Journal of Colloid and Interface Science, 363(2), 601–607.
27. Arora, C., Kumar, P., Soni, S., Mittal, J., Mittal, A., & Singh, B. (2020). Efficient removal of malachite green dye from aqueous solution using curcuma caesia based activated carbon. Desalination and Water Treatment, 195, 341–352.
28. Kumar, K. V. (2006). Comments on" Adsorption of acid dye onto organobentonite". Journal of hazardous materials, 137(1), 638-639.
29. Song, K., Xu, H., Xu, L., Xie, K., & Yang, Y. (2017). Cellulose nanocrystal-reinforced keratin bioadsorbent for effective removal of dyes from aqueous solution. Bioresource technology, 232, 254–262.

30. Fu, J., Chen, Z., Wang, M., Liu, S., Zhang, J., Zhang, J., ... & Xu, Q. (2015). Adsorption of methylene blue by a high-efficiency adsorbent (polydopamine microspheres): kinetics, isotherm, thermodynamics and mechanism analysis. Chemical Engineering Journal, 259, 53-61.
31. Wong, S., Tumari, H. H., Ngadi, N., Mohamed, N. B., Hassan, O., Mat, R., & Saidina Amin, N. A. (2019). Adsorption of anionic dyes on spent tea leaves modified with polyethyleneimine (PEI-STL). Journal of Cleaner Production, 206, 394–406.
32. Fahdil, A., Al-niaimi, D., & Muhi, F. H. (2019). Kinetic and Thermodynamic Study on the Removal of Congo Red from the Aqueous Solution Using Graphene Oxide / Magnesium Oxide Nanocomposite. 1–10.
33. Fahdil, Al-Niaimi, A. D., & Olaiwy, A. A. (2019). Removal Orange G dye from aqueous solutions using graphene oxide/magnesium oxide nano composite. International Journal of Research in Pharmacy and Chemistry, 9(1), 23-32.
34. Jaerger, S., Dos Santos, A., Fernandes, A. N., and Almeida, C. A. P. (2015). Removal of p-nitrophenol from aqueous solution using Brazilian peat: kinetic and thermodynamic studies. Water, Air, & Soil Pollution, 226(8), 236.
35. Olawale, S. A., & Okafor, C. C. (2020). Comparing the Different Methods Used in the Determination of Thermodynamic Parameters Using Adsorption of Pb (II) on to Chicken Feather as an Example. Jpurnal of Material Science an Reviews, 6(2), 1–11.
36. Errais, E., Duplay, J., Darragi, F., M'Rabet, I., Aubert, A., Huber, F., & Morvan, G. (2011). Efficient anionic dye adsorption on natural untreated clay: Kinetic study and thermodynamic parameters. Desalination, 275(1–3), 74–81.
37. Mahmoodi, N.M., Hayati, B., Bahrami, H. and Arami, M. (2011), "Dye Adsorption and Desorption Properties of Mentha pulegium in Single and Binary Systems". Journal of Applied Polymer Science, 122(3), pp: 1489-1499